Received: 28 October 2017 | Revised: 17 December 2017 | Accepted: 18 December 2017

DOI: 10.1002/chir.22822

SPECIAL ISSUE ARTICLE

WILEY

Comparison of measured and predicted specific optical rotation in gas and solution phases: A test for the polarizable continuum model of solvation

Tal Aharon[2] | Paul Lemler[1] | Patrick H. Vaccaro[1] | Marco Caricato[2]

[1] Department of Chemistry, Yale University, New Haven, Connecticut

[2] Department of Chemistry, University of Kansas, Lawrence, Kansas

Correspondence
Patrick H. Vaccaro, Department of Chemistry, Yale University, 225 Prospect St., New Haven, Connecticut 06511, USA.
Email: patrick.vaccaro@yale.edu

Marco Caricato, Department of Chemistry, University of Kansas, 1251 Wescoe Hall Dr., Lawrence, Kansas 66045, USA.
Email: mcaricato@ku.edu

Funding information
National Science Foundation, Grant/Award Number: CHE-1650942; U.S. National Science Foundation, Grant/Award Number: CHE-1464957

Abstract

A comparative theoretical and experimental study of dispersive optical activity is presented for a set of small, rigid organic molecules in gas and solution phases. Target species were chosen to facilitate wavelength-resolved measurements of specific rotation in rarefied vapors and in organic solvents having different polarities, while avoiding complications due to conformational flexibility. Calculations were performed with two density functionals (B3LYP and CAM-B3LYP) and with the coupled-cluster singles and doubles (CCSD) ansatz, and solvent effects were included through use of the polarizable continuum model (PCM). Across the various theoretical methods surveyed, CCSD with the modified velocity gauge provided the best overall performance for both isolated and solvated conditions. Zero-point vibrational corrections to equilibrium calculations of chiroptical response tended to improve agreement with gas-phase experiments, but the quality of performance realized for solutions varied markedly. Direct comparison of measured and predicted specific-rotation suggests that PCM, in general, is not able to reproduce attendant solvent shifts (neither between gas and solution phases nor among solvents) and fares better in estimating actual medium-dependent values of this property (although the error is rather system dependent). Thus, more elaborate solvation models seem necessary for a proper theoretical description of solvation in dispersive optical activity.

KEYWORDS

benchmark, CRDP, PCM, quantum chemistry, solvation, specific rotation

1 | INTRODUCTION

The study of chiroptical properties has been of great importance since the discovery of optical activity in crystals by Arago (1811) and Biot (1812), with continuing interest being due, in part, to the pervasive nature of chiral species in biochemical science and the pharmaceutical industry.[1] Since the specific optical rotation, $[\alpha]_{\lambda}^{T}$ (at wavelength λ and temperature T), of chiral molecules is tied closely to their absolute stereochemical configuration, which, in turn, often determines their pharmacological activity, ab initio studies of this fundamental quantity have become increasingly popular as they can provide direct access to a key structure-property correlation. Beginning with the work of Polavarapu in 1997 at the Hartree-Fock level of theory, quantum-

chemical calculations of specific rotation have been extended to density functional theory (DFT) and to coupled cluster theory (CC).[2-15]

Although the aforementioned theoretical approaches successfully have aided in the characterization of chiral molecules and their interactions, open questions remain. One key issue is the ability to reproduce the effects of solvation on observed specific-rotation values. The work of the Vaccaro group on the measurement of dispersive chiroptical signatures in the vapor phase by means of cavity ring-down polarimetry (CRDP) has revealed unexpectedly large changes in the magnitude and even the sign of $[\alpha]_\lambda^T$ upon transferring chiral species from the vacuum to the condensed phase.[16-22] Despite extensive efforts, such large effects have eluded a robust theoretical characterization.

Several theoretical methods to approximate the effects of solvent upon $[\alpha]_\lambda^T$ have been reported. By combining continuum solvation models and molecular dynamics simulations, Mukhopadhyay et al. managed to obtain qualitative agreement with experimental data acquired for a simple chiral test molecule, methyloxirane. Their analyses showed that the optical rotation in water was dominated by the solute contribution, while the dissymmetric first solvation shell formed in a benzene solvent contributed nearly as much to the specific rotation as the solute itself.[23,24] Kundrat et al. utilized molecular dynamics simulations to evaluate specific rotations for a series of amino acids. These authors used explicit point charges to approximate solvent molecules in quantum-mechanical calculations created from classical-dynamics snapshots and compared emerging results to those obtained from a continuum-solvation model. They attributed the poorer performance of the explicit solvation approach in reproducing the experimental $[\alpha]_\lambda^T$ values to shortcomings of DFT.[25,26] Crawford and co-workers[17] applied CC calculations for the solute with frozen-density embedding potentials for the solvent, but this approach was not sufficient to reproduce the solvation effect on specific rotation correctly, despite previous success with electronic absorption spectra. Haghdani et al[27] used a microsolvation-plus-continuum scheme to calculate specific rotation in solution but concluded that further developments were needed to quantitatively predict solvation effects. Other work has entailed use of polarizable force fields to describe the solvent, which showed promise for describing the change in sign of methyloxirane rotation observed in solution phases.[28] However, these approaches were unable to account consistently and generally for solvation effects on specific rotation, and they also required considerable computational effort as they all are based on multiple $[\alpha]_\lambda^T$ evaluations for tens or hundreds of snapshots derived from molecular dynamics simulations.

Another approach to describe solvation effects is based on continuum models, where the atomistic representation of the solvent is replaced by a continuous, polarizable medium. These methods provide considerable computational savings as they avoid the need for conformational sampling. One of the most widely used schemes is the polarizable continuum model (PCM) developed by Tomasi and co-workers.[29-32] Indeed, preliminary DFT-PCM studies have shown some success in reproducing solvent effects on $[\alpha]_\lambda^T$, suggesting that this may be an efficient scheme for predicting specific optical rotation in the condensed phase.[33-35] Recent efforts combining the linear response-CC (LR-CC) approach and PCM also have provided some encouraging results.[36] The present contribution systematically investigates the ability of PCM to reproduce solvent effects on the dispersive chiroptical properties exhibited by a series of conformationally rigid chiral molecules and affords a thorough comparison of calculated and experimental values of specific optical rotation across multiple wavelengths and phases (viz., in the vapor phase and in various solvents possessing distinct polarities). In contrast to recent studies focusing on anomalously large rotatory powers imbued by the action of inherently dissymmetric chromophores, the ensuing analyses have addressed the more typical case of modest optical activities resulting from localized stereogenic elements that are perturbed asymmetrically by the surrounding chemical environment.[37,38] Zero-point vibrational corrections (ZPVCs) also are evaluated in the gas and solution phases, as they have been shown to be capable of significantly modifying the purely electronic response, and may be a dominating factor in the temperature dependance of the specific rotation.[39-42]

Measurements and calculations of specific rotation in both gas and solution phases are presented for a set of four molecules: (*R*)-α-pinene (**1**), (*S*)-3-carene (**2**), (*R*)-*cis*-pinane (**3**), and (*S*)-2-chloropropionitrile (**4**), the structures of which are shown in Figure 1. These compounds were chosen for their volatility and relative magnitude of rotation (which facilitate measurements in the vapor phase), for their solubility in organic solvents, and for their conformational rigidity (which avoids contributions from several isomers that would complicate comparisons between theory and experiment). The solvents selected

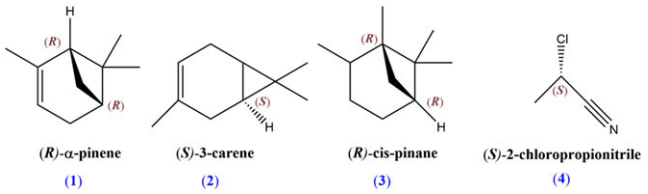

FIGURE 1 The set of chiral molecules targeted by the present study

TABLE 1 Solvents used in this work, and their optical (ε_∞) and static (ε_0) dielectric constants

Solvent	ε_∞	ε_o
Acetonitrile (ACN)	1.81	35.7
Methanol (MOH)	1.77	32.6
Chloroform (CHL)	2.09	4.7
Dibutyl Ether (DBE)	1.96	3.0
Benzene (BNZ)	2.25	2.3
Cyclohexane (CYH)	2.04	2.0

for the present study are listed in Table 1, along with their static (ε_0) and optical (ε_∞) dielectric constants, which are the main parameters used in the PCM treatment of solvation.

2 | MATERIALS AND METHODS

2.1 | Theory and computational details

Calculations of $[\alpha]_\lambda^T$, expressed in deg dm^{-1} (g/mL)$^{-1}$, are reported, with the equilibrium values of these quantities (vide infra) being evaluated as:

$$[\alpha]_\lambda = \frac{1.92\cdot 10^{14}\pi^2 N_A a_0^4}{M\lambda^2} Tr\left(\boldsymbol{G}'\right), \tag{1}$$

where N_A is the Avogadro constant, a_0 is the Bohr radius in cm, λ is the wavelength of the incident light in nm, and M is the molecular weight of the chiral molecule in g/mol. Here $\boldsymbol{G}'$ is the mixed electric dipole-magnetic dipole polarizability tensor, or Rosenfeld tensor, which is computed by using standard linear-response techniques.[43-46] Zero-point vibrational corrections (ZPVCs) are evaluated by using a Taylor-series expansion of the specific rotation about the equilibrium geometry of the molecule:

$$[\alpha]_\lambda^T \approx [\alpha]_\lambda^{eq} + \frac{1}{2}\sum_{i=1}^{3N-6} \frac{\partial^2 [\alpha]_\lambda^{eq}}{\partial {Q_i}^2} \langle \Delta x_i \rangle_T^2, \tag{2}$$

where $[\alpha]_\lambda^{eq}$ is the specific rotation at the equilibrium geometry as defined by Equation 1. This expansion neglects the first derivative of specific rotation with respect to the normal modes;[41] however, computation of this missing term also requires the evaluation of cubic force constants, which was deemed too demanding in the context of the present work. Therefore, the ZPVCs in Equation 2 are limited to quadratic terms as this should be sufficient for a semiquantitative discussion of the results. The sum in Equation 2 runs over the harmonic vibrational degrees of freedom of the molecule, with the square of the average thermal displacement along the ith normal mode, $\langle \Delta x_i \rangle_T$, being given by:

$$\langle \Delta x_i \rangle_T^2 = \left(\frac{16.8576}{\widetilde{\nu}_i}\right) \coth \frac{0.719384\widetilde{\nu}_i}{T}, \tag{3}$$

where $\widetilde{\nu}_i$ is the fundamental wavenumber (in cm^{-1}) for the ith vibrational displacement.[40] Only corrections at 0K are considered, as this again is enough for a semiquantitative discussion. The second derivative of the specific rotation in Equation 2 is approximated as:

$$\frac{\partial^2 [\alpha]_\lambda^{eq}}{\partial {Q_i}^2} \approx \frac{[\alpha]_\lambda^{+\delta_i} - 2[\alpha]_\lambda^{eq} + [\alpha]_\lambda^{-\delta_i}}{\delta_i^2}. \tag{4}$$

Here the mass-weighted displacement δ_i is obtained by normal-mode scaling:

$$\delta_i = \frac{Q_i s}{\sqrt{\widetilde{\nu}_i}}, \tag{5}$$

where $s = 0.1$ follows from the recommendation of Crawford and coworkers, and the square root of the vibrational frequency in the denominator (in analogy to the average displacement in Equation 3) is introduced to produce larger displacements for soft modes.[47]

All calculations were performed with a development version of the GAUSSIAN suite of programs.[48] Optimized geometries obtained by applying the B3LYP/aug-cc-pVTZ model chemistry in each respective medium (i.e., gas phase and solution phase) were used for specific-rotation calculations with all other levels of theory to avoid geometrical effects. The $[\alpha]_\lambda^T$ calculations were performed with the aug-cc-pVDZ basis set, which offers a good compromise between computational accuracy and cost, at the following levels of theory: B3LYP, CAM-B3LYP, and coupled-cluster singles and doubles (CCSD).[49-57] The DFT methods exploited the length gauge with gauge-including atomic orbitals to remove origin dependence.[14,58,59] Since gauge-including atomic orbitals cannot be used with standard CCSD, calculations are reported for the modified velocity gauge (MVG, origin independent) and the length gauge (LG, origin dependent) because the latter has shown better convergence with basis-set size.[12] All ZPVC calculations were performed with B3LYP, and the results were added to the equilibrium $[\alpha]_\lambda^T$ values computed at other levels of theory.

Calculations in solution used the symmetric integral equation formalism version of PCM (but denoted as "PCM" in the following text).[60] In this model, the solvent is represented by a continuous and polarizable medium where a cavity of proper molecular shape hosts the solute. The solute-solvent electrostatic interaction is introduced through an effective term in the Hamiltonian, which depends on the macroscopic static dielectric constant, ε_0. PCM also can be used to introduce solvent effects on

frequency-dependent molecular properties such as the specific rotation.[29,32] These calculations are performed in the nonequilibrium regime, which assumes that the solvent molecules and nuclei are too slow to respond to changes in the solute electron density and are kept fixed (i.e., the inertial response), while the solvent electrons respond instantaneously (i.e., the dynamic response). The latter enters the solute linear-response equations used to evaluate the Rosenfeld tensor, and the PCM term now depends on the optical dielectric constant of the solvent, ε_∞ (i.e., the square of the refractive index). The cavity is built as a series of interlocking spheres centered on the solute nuclei and the radii are parameterized. Based on preliminary tests, cavities were built with Bondi radii and a scaling factor of 1.2 (viz., $R_C = 1.7$ Å, $R_H = 1.2$ Å, $R_N = 1.55$ Å, and $R_{Cl} = 1.75$ Å). Added spheres have been used for the specific rotation calculations to avoid unphysical solvent pockets. Zero-point vibrational correction calculations were performed by maintaining the cavity fixed during numerical differentiation (cf. Equation 4), as initial tests showed numerical instabilities when the cavity was moved during the geometry displacements.

3 | EXPERIMENTAL DETAILS

Experimental values of specific optical rotation, $[\alpha]_\lambda^T$ in deg dm^{-1} $(g/ml)^{-1}$, at incident wavelength λ and near-ambient temperature T were obtained, in part, from published CRDP studies, which gave requisite intrinsic (vapor-phase) chiroptical properties for (*R*)-α-pinene (**1**),[18] (*S*)-3-carene(**2**),[22] (*R*)-*cis*-pinane (**3**),[18] and (*S*)-2-chloropropionitrile[21] (**4**) at $\lambda = 355$ nm and $\lambda = 633$ nm. Complementary solvated quantities for **4** were acquired from the same source, while new solution-phase measurements were performed for other targeted species.[21]

Samples of **1**, **2**, and **3** were procured from a commercial source (*Sigma-Aldrich*) and used without further processing at their specified purities of 99%, 99%, and 98.5%. While **1** was stated by the manufacturer to have a percentage enantiomeric excess (%ee) of 97%, neat optical rotation measurements for **2** at the sodium D-Line (589.3 nm) suggested >97% ee when compared to previously published metrics and chiral GC-MS analyses of **3** (based on a *Sigma-Aldrich* B-DM column; 40 m length x 0.25 mm diameter) indicated >95% ee.[22] As such, explicit corrections of measured $[\alpha]_\lambda^T$ parameters for enantiomeric and chemical purity were deemed to be unnecessary.

Solution-phase studies of dispersive optical activity were performed in a temperature-regulated (25 ± 1 °C) quartz sample cell (10.000 ± 0.005 cm length) by utilizing a commercial polarimeter (*Perkin-Elmer* 241; ±0.002° angular accuracy) that operated at discrete visible/ultraviolet excitation wavelengths filtered from NaI and HgI atomic-emission lamps (viz., 365.02, 436.83, 546.07, 578.39, and 589.30 nm). Each measurement was repeated at least twice with a substantial integration time (20 s) being used to ensure reproducibility, leading to reported quantities that represent the average of acquired experimental results. Solvents selected for the present study, acetonitrile (ACN), methanol (MOH), chloroform (CHL), di-*n*-butyl ether (DBE), benzene (BNZ) and cyclohexane (CYH), were of spectrometric grade, and solute concentrations were kept as low as possible (typically $\leq 10^{-3}$ g/mL) to minimize aggregation (solute-solute) effects while still retaining high polarimetric precision.

Since intrinsic rotatory powers were restricted to excitation wavelengths that did not overlap with those available for solution-phase measurements, solvated results were extrapolated to their vapor-phase counterparts by performing nonlinear least squares regressions based on the following functional form:

$$[\alpha]_\lambda^T = A\left(\frac{2\gamma_{eg}\lambda_{eg}}{\left(\lambda_{eg}-\gamma_{eg}\right)^2}\right)\frac{2\lambda_{eg}^2\left[\lambda^2-\lambda_{eg}^2-\left(\frac{\lambda\lambda_{eg}}{\gamma_{eg}}\right)^2\right]}{\left[\left(\lambda-\lambda_{eg}\right)^2+\left(\frac{\lambda\lambda_{eg}}{\gamma_{eg}}\right)^2\right]\left[\left(\lambda+\lambda_{eg}\right)^2+\left(\frac{\lambda\lambda_{eg}}{\gamma_{eg}}\right)^2\right]} \quad (6)$$

where A is an overall amplitude factor while λ_{eg} and γ_{eg} denote the resonant wavelength and spectral dephasing linewidth for an isolated electronic transition between excited state $|e\rangle$ and ground state $|g\rangle$. For an $|e\rangle \leftrightarrow |g\rangle$ resonance characterized by dephasing rate $\Gamma_{eg} = 1/\tau$ (in s^{-1}), where τ (in s) denotes the corresponding dephasing time, the quantity γ_{eg} (in m) is related formally through the speed of light in a vacuum, c, as $\gamma_{eg} = 2\pi c/\Gamma_{eg} = 2\pi c\tau$. Deduced from a full perturbative expansion for attendant matter-field interactions, this expression correctly predicts the vanishing magnitude of specific rotation in the asymptotic limit of long wavelengths ($\lambda \to \infty$).[16] In view of the 3 adjustable parameters (A, λ_{eg} and γ_{eg}) in Equation 6, attempts to utilize this model directly for the least squares interpolation of vapor-phase measurements were hindered by the availability of only 2 data points (at 355 and 633 nm). Under such circumstances, the value of A was constrained to equal that obtained from analyses of the closest solution-phase mimic for isolated-molecule behavior (often acetonitrile).

4 | RESULTS AND DISCUSSION

The optical-activity results are presented as a series of correlation plots between experiment and theory. Two

quantities of particular interest are considered: the equilibrium value of the specific rotation, $[\alpha]_\lambda^T$, and the attendant solvation shift, $\Delta[\alpha]_\lambda^T$, defined by:

$$\Delta[\alpha]_\lambda^T = [\alpha]_{\lambda,\text{solv}}^T - [\alpha]_{\lambda,\text{gas}}^T. \quad (7)$$

Zero-point vibrational corrections only are considered in a second stage because the effects on $\Delta[\alpha]_\lambda^T$ are large and would complicate the discussion. The aforementioned $[\alpha]_\lambda^T$ and $\Delta[\alpha]_\lambda^T$ plots are presented separately for each molecule and level of theory, with the $[\alpha]_\lambda^T$ results (gas and solution phase) for all wavelengths reported on the same graph. In this way, the performance across various media can be assessed readily via visual inspection. All numerical values are listed in Tables S26–S65 in the supporting information. Four key wavelengths are examined in detail by the present study: 355, 436.83, 589.3, and 633 nm, where 355 and 633 nm are the incident wavelengths available for gas-phase CRDP measurements, while 436.83 and 589.3 nm are two of the emission lines used for solution-phase measurements. Phase-dependent values of specific rotation at wavelengths for which measurements are not available are obtained from the least squares regression procedure described in section 3 (cf. Equation 6). Experimental findings are reported along the horizontal axis, while the corresponding calculated quantities are reported along the vertical axis. In addition, two linear fits of each dataset have been performed, one for the gas phase and one for the solution phase (the latter considering all solvents concurrently).

Figure 2 displays optical-activity results for compound **1**. Experimentally, $[\alpha]_\lambda^T$ decreases when going from a rarefied gaseous medium to the condensed (solution) phase, except in methanol, for which it increases. The slope of the CAM-B3LYP linear fit shows a nearly 1:1 correspondence between theory and experiment for the gas phase, with experiment being overpredicted for the solution phase. B3LYP and CCSD-LG underestimate both gas and solution phase measurements. Coupled-cluster singles and doubles with the modified velocity gauge calculations predict $[\alpha]_\lambda^T$ values that are too low in the gas phase but reproduce solution-phase measurements rather well. The trends across solvents obtained from CCSD-LG and both DFT methods are contradictory to what is found in experiments. For instance, the calculated solvent effects for acetonitrile and chloroform are large, while the experimental shifts are small (measured 355 nm values of 188.2, 186.6, and 188.8 deg dm^{-1} [g/mL]$^{-1}$ in gas, ACN, and CHL). In addition, experiments performed in benzene, cyclohexane, dibutyl ether, and methanol show a significant change, amounting to between 10% and 20% of the gas phase value (measured 355 nm values of 188.2,

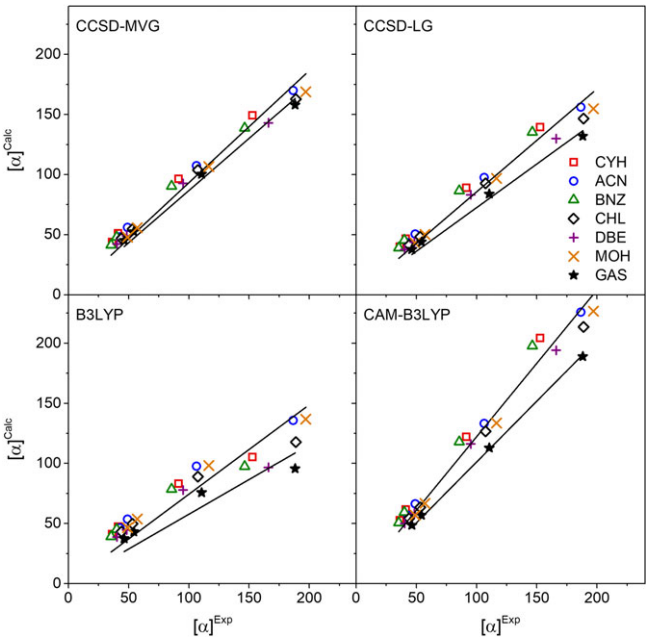

FIGURE 2 Gas and solution phase plots of $[\alpha]_\lambda^T$ (in deg dm^{-1} [g/mL]$^{-1}$) for (*R*)-α-pinene (**1**). The solvent acronyms are listed in Table 1

146.3, 152.8, 166.0, and 197.1 deg dm^{-1} [g/mL]$^{-1}$ in gas, BNZ, CYH, DBE, and MOH), while the best predicted shifts for the same solvents, obtained with PCM and CCSD-MVG, range between 5% and 10% (CCSD-MVG 355 nm values of 157.9, 138.7, 152.8, 143.0, and 168.8 deg dm^{-1} [g/mL]$^{-1}$ in gas, BNZ, CYH, DBE, and MOH). The experimental $[\alpha]_\lambda^T$ parameters decrease in magnitude from acetonitrile to benzene in order of decreasing ε_0 and increasing ε_∞ (cf. Table 1). In all calculations, this ranking is maintained for acetonitrile, cyclohexane, and benzene but not for dibutyl ether and methanol. While the correlation between experimental and calculated rotatory powers increases linearly with decreasing wavelength for CCSD and CAM-B3LYP, the B3LYP data points deviate markedly from linearity.

For compound **2**, Figure 3 reveals large differences between gas-phase and solution-phase results. The correlation plots show very good agreement for gas-phase rotatory powers across all methods, although experimental values consistently are underestimated. Similarly, the comparison between theory and experiment for solvated response is fairly linear across all methods; however, predicted values generally overestimate observed behavior. Interestingly, the experimental findings suggest a large shift in $[\alpha]_\lambda^T$ between isolated and solvated conditions, indicating the action of a general "solvation" shift that is nearly independent of the choice of solvent. The relative change in magnitude between gas-phase chiroptical response and that of the closest-lying solvent, dibutyl

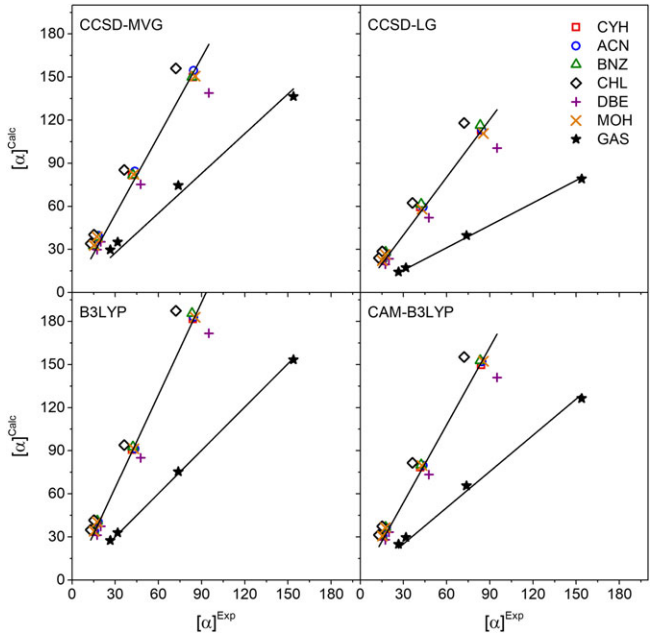

FIGURE 3 Gas and solution phase plots of $[\alpha]_\lambda^T$ (deg dm^{-1} [g/mL]$^{-1}$) for (*S*)-3-carene (**2**). The solvent acronyms are listed in Table 1

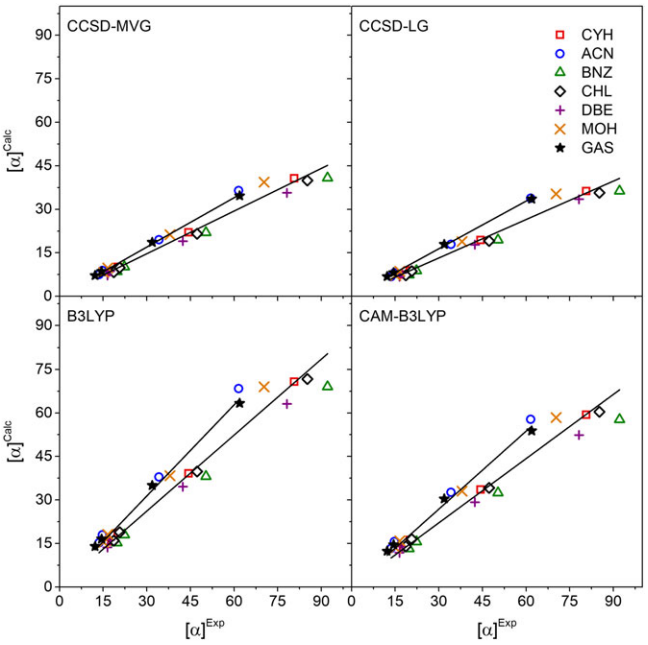

FIGURE 4 Gas and solution phase plots of $[\alpha]_\lambda^T$ (deg dm^{-1} [g/mL]$^{-1}$) for (*R*)-*cis*-pinane (**3**). The solvent acronyms are listed in Table 1

ether, is 5 times greater than the largest difference between 2 solvents (measured 355 nm values of 153.8, 85.5, and 72.1 deg dm^{-1} [g/mL]$^{-1}$ in gas, DBE, and CHL). The sign of this shift is not in keeping with calculations, which suggest $[\alpha]_\lambda^T$ to be larger in solution than in the gas phase (cf. ensuing discussion and $[\alpha]_\lambda^T$ plots). Experimental solvent trends also are not reproduced, as the medium with the largest observed rotatory powers, dibutyl ether, has the smallest predicted $[\alpha]_\lambda^T$ values (across all methods), while the opposite behavior is obtained for chloroform.

The calculated and experimental $[\alpha]_\lambda^T$ parameters for compound **3** are highlighted in Figure 4. As with the previous systems, the correlation between theory and experiment under rarified conditions is quite good, with DFT showing particularly strong results indicated by a linear slope near unity. In solution, experimental values are dispersed in a manner that is not reproduced by the calculations. The solvent-induced perturbation is small in acetonitrile, where the specific rotation is nearly identical to that of the gas phase, and becomes quite large in benzene, where the effective shift represents 50% of the gas-phase results (measured 355 nm values of 61.9, 61.6, and 92.1 deg dm^{-1} [g/mL]$^{-1}$ in gas, ACN, and BNZ). Coupled-cluster singles and doubles with the modified velocity gauge predicts that the effect of acetonitrile to be very small and, while the largest change from gas to any solvent still is obtained with benzene, the magnitude of this effect is reduced to only 20% (CCSD-MVG 355 nm values of 34.7, 36.5, and 40.8 deg dm^{-1} [g/mL]$^{-1}$ in gas, ACN, and BNZ). Density functional theory also predicts very small shifts with PCM, amounting to only 10% from gas to benzene in the case of B3LYP (B3LYP 355 nm values of 63.3 and 69.1 deg dm^{-1} [g/mL]$^{-1}$ in gas and BZN). The largest difference in rotatory powers now is between two solvents, chloroform and dibutyl ether, rather than with the gas phase (B3LYP 355 nm values of 70.7 and 63.1 deg dm^{-1} [g/mL]$^{-1}$ in CHL and DBE).

Figure 5 illustrates results obtained for compound **4**, which is the only chiral system having a negative optical rotation in the current dataset. Studies performed in benzene are not included, as they seem to exhibit behavior inconsistent with those of other solvents and molecules. Linear correlation plots obtained for the CCSD-MVG gas-phase and solution-phase predictions have nearly identical slopes, which probably is fortuitous given the spread of the experimental results in solution, while other methods yield gas-phase slopes greater than their solution-phase counterparts. The three latter methods also predict acetonitrile rotatory powers to fall essentially along the linear fit of the gas phase. In addition, while the observed range of solvated chiroptical response is appreciable (measured 355 nm values of −45.4 and −64.4 deg dm^{-1} [g/mL]$^{-1}$ in ACN and CYH), there is very little difference between any pair of solvents in the calculations (the largest being found for CCSD-MVG which yields 355 nm predictions of −38.7 and −42.7 deg dm^{-1} [g/mL]$^{-1}$ in MOH and CYH). Nevertheless, quantum-chemical analyses reproduce the qualitative trends seen in the experiments, where $[\alpha]_\lambda^T$ is largest for cyclohexane, followed by dibutyl ether and then

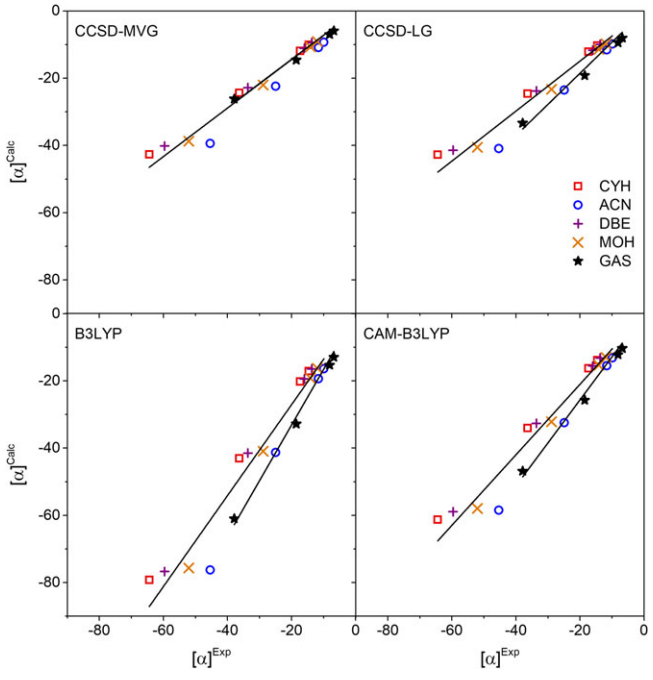

FIGURE 5 Gas and solution phase plots of $[\alpha]_\lambda^T$ (deg dm^{-1} [g/mL]$^{-1}$) for (*S*)-2-chloropropionitrile (**4**). The solvent acronyms are listed in Table 1

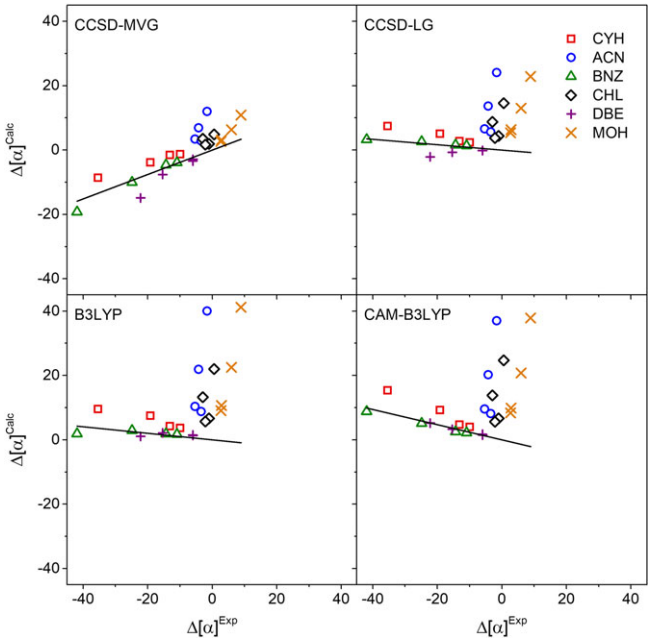

FIGURE 6 The $\Delta[\alpha]_\lambda^T$ plots (deg dm^{-1} [g/mL]$^{-1}$) for (*R*)-α-pinene (**1**). The solvent acronyms are listed in Table 1

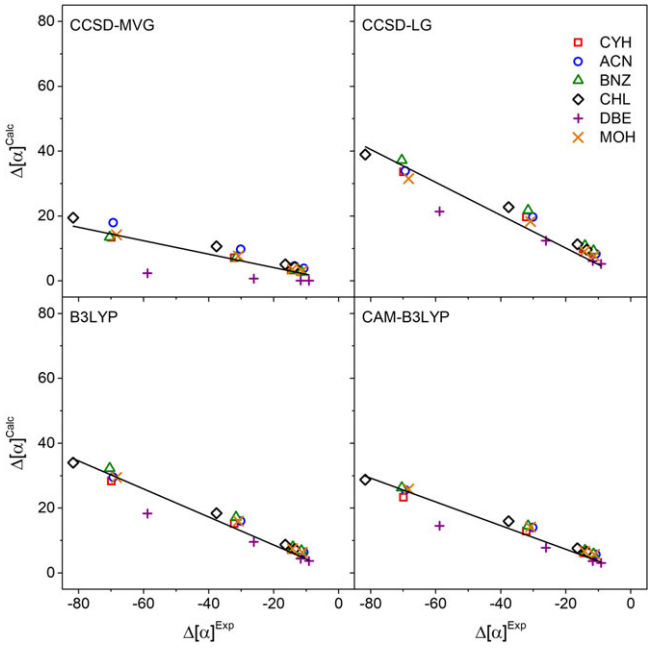

FIGURE 7 The $\Delta[\alpha]_\lambda^T$ (deg dm^{-1} [g/mL]$^{-1}$) plots for (*S*)-3-carene (**2**). The solvent acronyms are listed in Table 1

methanol, although acetonitrile does not fit this trend. The magnitude of the solution-phase specific rotation increases with increasing ε_∞ in the calculations, and with decreasing ε_0 in the experiments, but the two sequences are different, as depicted in Table 1.

We now move to a discussion of solvent shifts, $\Delta[\alpha]_\lambda^T$, the first of which is presented in Figure 6 for molecule **1**. In contrast to other methods, CCSD-MVG successfully reproduces the proper sign of this quantity for cyclohexane, benzene, and dibutyl ether, but the magnitude is underestimated by a nearly a factor of two. The $\Delta[\alpha]_\lambda^T$ values predicted by CCSD-MVG for methanol also have the same sign as the experimental values and are reproduced nearly quantitatively as well. The signs of $\Delta[\alpha]_\lambda^T$ estimated by CCSD-MVG for acetonitrile and chloroform are incorrect, although experimental values are difficult to reproduce as their magnitude is smaller than the expected accuracy of the theoretical methods (experimental [CCSD-MVG] 355 nm values of −1.6 [12.0] and 0.6 [4.9] deg dm^{-1} [g/mL]$^{-1}$ in ACN and CYH). The largest shift both experimentally and theoretically is observed for benzene. All other theoretical approaches predict incorrect signs for the solvent shifts.

The solvent shifts for compound **2** are illustrated in Figure 7. In addition to the overprediction of solvent effects mentioned above, experiments and calculations also disagree on the direction of the shifts, with the former displaying a negative slope while the latter predict solvation to increase the magnitude of $\Delta[\alpha]_\lambda^T$. Additionally, CCSD-LG and both DFT methods yield very similar $\Delta[\alpha]_\lambda^T$ parameters, while CCSD-MVG suggests much smaller values.

Figure 8 highlights the $\Delta[\alpha]_\lambda^T$ results obtained for compound **3**. The calculations reproduce the sign of the experimental shift (except in the case of acetonitrile), but the

magnitude is severely underestimated. Despite an incorrect sign, both choices of gauge for CCSD correctly predict a very small shift in acetonitrile (355 nm shift values of −0.3, 1.8, and 0.2 deg dm^{-1} $[g/mL]^{-1}$ by experiment, CCSD-MVG, and CCSD-LG). The CC methods also duplicate the smaller shift observed in chloroform than in benzene while erroneously giving a greater shift in cyclohexane than in chloroform. The converse is true for DFT, where the acetonitrile results are large (355 nm shift values of 5.1 and 3.9 deg dm^{-1} $[g/mL]^{-1}$ by B3LYP and CAM-B3LYP), the benzene shift is smaller than that of chloroform, and $\Delta[\alpha]^{T}_{\lambda}$ in chloroform is larger than in cyclohexane (as found in the experiments).

Figure 9 depicts the $\Delta[\alpha]^{T}_{\lambda}$ results for compound **4**. Although the shift magnitudes are underestimated by calculations, particularly by CCSD-LG, the correct sign is obtained. Despite the nonlinear trend noted for acetonitrile, which arises from the small experimental change of $\Delta[\alpha]^{T}_{\lambda}$ with wavelength relative to calculated values, calculations for all solvents produce similar shifts. This anomaly may stem from the similar structures of acetonitrile and **4**, which could lead to subtle interactions that differ from those operating in other (bulkier) solvents. Such effects are not reproduced by PCM since the atomistic nature of the solvent is neglected. To a lesser extent, this also is true for methanol, which exhibits comparable behavior. The trend reported for the $[\alpha]^{T}_{\lambda}$ plots of **4** in Figure 5, where the magnitude of the specific rotation in solution increases with increasing ε_{∞} in calculations and with decreasing ε_0 in experiments, is present in the $\Delta[\alpha]^{T}_{\lambda}$ shifts as well.

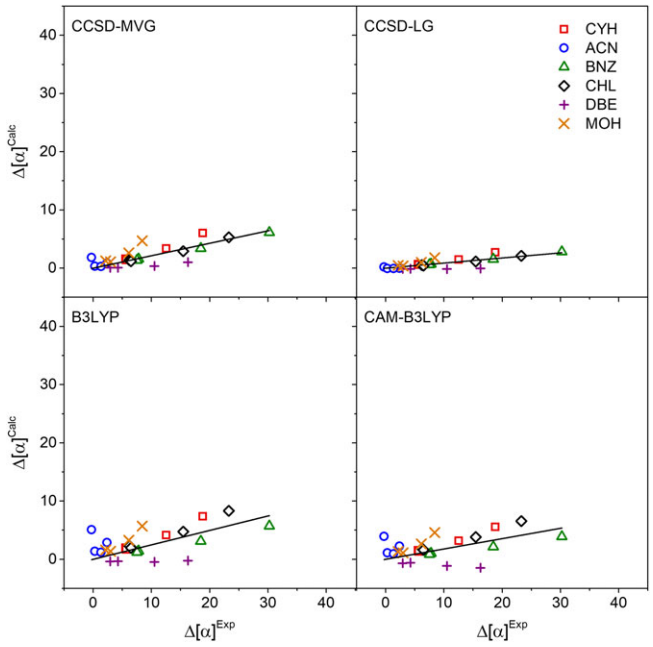

FIGURE 8 The $\Delta[\alpha]^{T}_{\lambda}$ (deg dm^{-1} $[g/mL]^{-1}$) plots for (*R*)-*cis*-pinane (**3**). The solvent acronyms are listed in Table 1

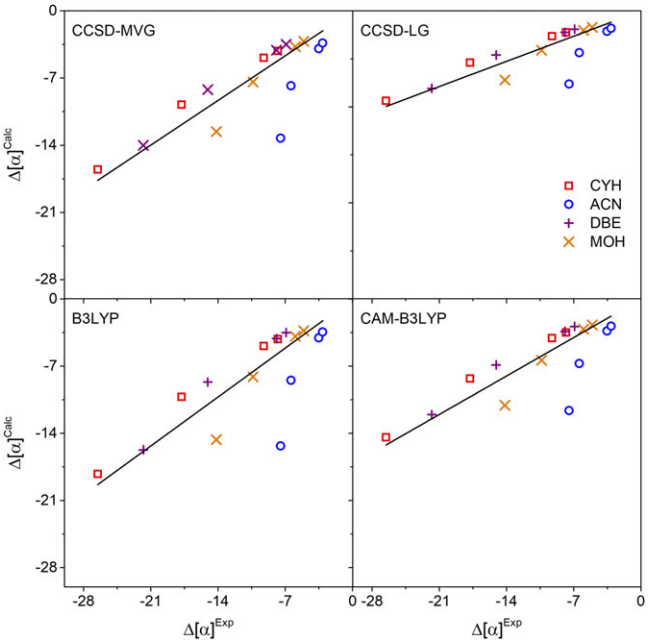

FIGURE 9 The $\Delta[\alpha]^{T}_{\lambda}$ (deg dm^{-1} $[g/mL]^{-1}$) plots for (*S*)-2-chloropropionitrile (**4**). The solvent acronyms are listed in Table 1

The trends across molecules can be compared directly by examining the R^2 (correlation coefficient) metrics and attendant slopes extracted from linear regressions in Figures 2–9 (where intercepts were constrained to zero). These results have been compiled in Figures 10 (gas phase) and 11 (solution phase), with the corresponding ZPVCs, as discussed in section 2.1, also being included. Excellent agreement is achieved between experiment and theory in the gas phase. The R^2 values indicate a strong linear correlation to exist between the calculated and experimental rotatory powers, while the accompanying near-unity slopes imply the former to reproduce the latter uniformly. The CCSD-MVG method performs exceptionally well for compounds **1**, **2,** and **4** but underestimates experiments for **3**. The CAM-B3LYP slopes are close to unity for **1**, **2**, and **3**, suggesting good predictions of polarimetric results, while the slope for molecule **4** is significantly larger than that for **1**. As shown in Figure 10, vibrational corrections tend to improve calculations by enhancing the quality of correlation attained with measurements. However, because the addition of ZPVCs consistently increases the slope for these systems, analyses that underestimate this quantity are improved while those that do not are made worse. Consequently, the consistently underpredicted CCSD-LG slopes are enhanced towards unity while their overpredicted CAM-B3LYP counterparts always deteriorate upon addition of ZPVCs. The performance of B3LYP and CCSD-MVG with ZPVCs depends on how well experimental values are duplicated initially, although such corrections do tend to improve the overall agreement with experiment.

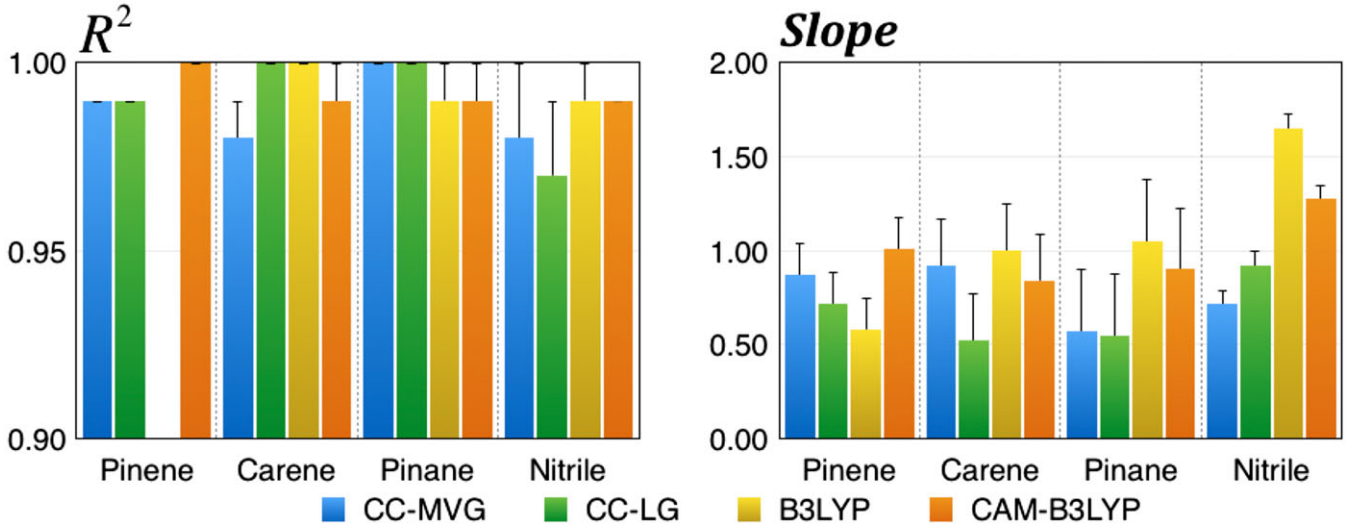

FIGURE 10 The R^2 coefficients and slopes for linear fits of the gas-phase specific rotation. The black bars indicate how the values change when zero-point vibrational corrections (ZPVCs) are included

The R^2 metrics for solution-phase specific rotations in Figure 11 suggest that the linear correlation between experiment and theory remains reasonable, although not as good as in the gas phase. Indeed, the accompanying slopes imply that solvated results depend strongly on the solute being considered. Coupled-cluster singles and doubles methods consistently underestimate experimental findings, except for **2**, which (as mentioned previously) would appear to be an especially difficult case. For compound **1**, slopes from either choice of gauge for CCSD are just under unity, while those for **3** and **4** are much smaller than unity. Density functional theory methods have similar difficulties predicting $[\alpha]_\lambda^T$ for **2**, but also tend to overestimate or underestimate rotatory powers for the remaining three molecules without a clear pattern. Zero-point vibrational corrections improve the quality of correlation attained for **1** and **2**, while worsening it for the other two species of interest. Such corrections tend to increase the slope of the linear fit obtained for all methods and molecules, thus (as found in the gas-phase) enhancing the performance of methods that underpredict experiments while diminishing that of their over-predicting counterparts.

Figure 12 contains the R^2 (correlation-coefficient) metrics and slopes extracted from consideration of solvent shifts, both of which suggest the correlation between experiment and theory to be exceptionally weak. The R^2 parameters for plots of **2** are much better than those of

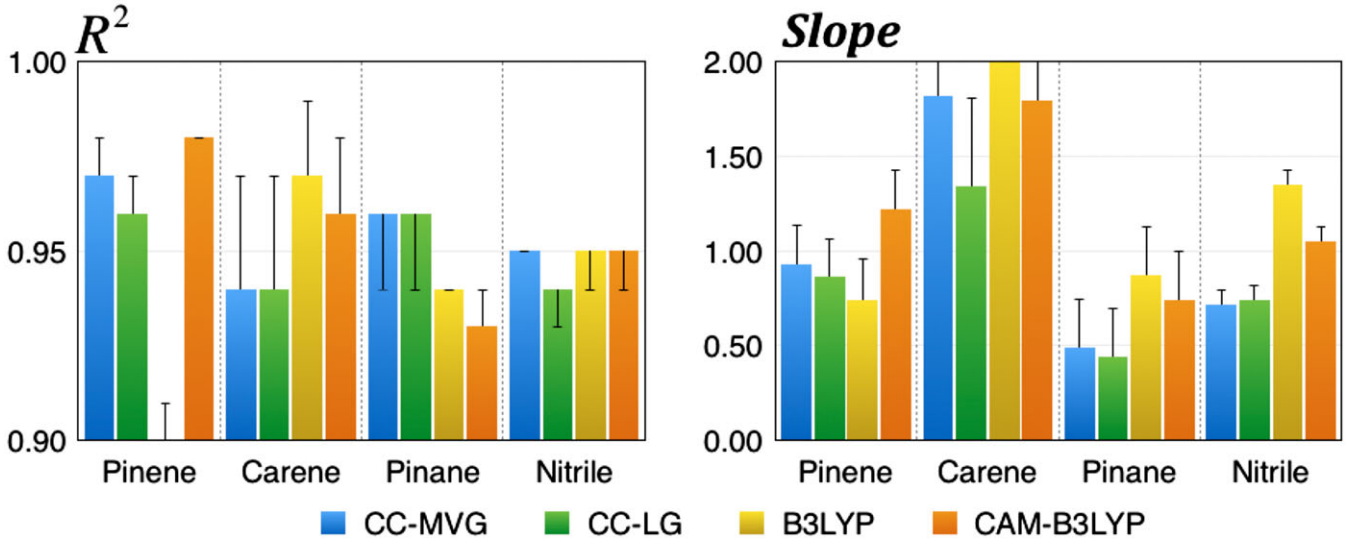

FIGURE 11 The R^2 coefficients and slopes for the linear fits of the solution-phase specific rotation. The black bars indicate how the values change when zero-point vibrational corrections (ZPVCs) are included

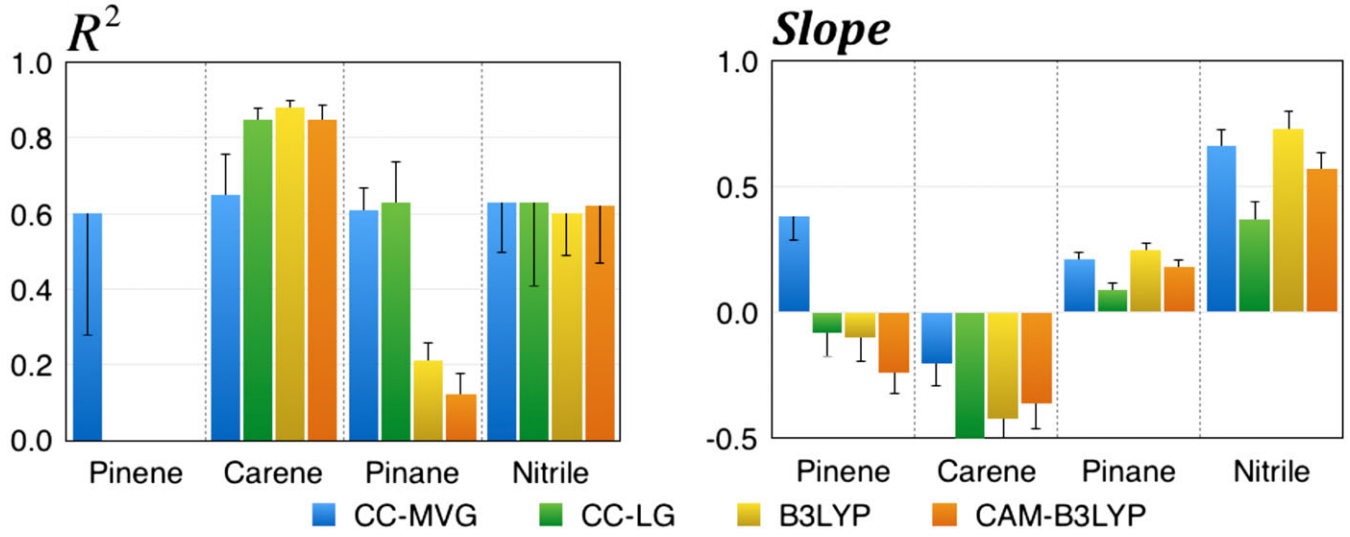

FIGURE 12 The R^2 coefficients and slopes for the linear fits of the solvent shifts. The black bars indicate how the values change when zero-point vibrational corrections (ZPVCs) are included. The R^2 values for (*R*)-α-pinene are negative (not reported), which is indicative of very weak correlation between data points

the other solutes, yet calculations predict corresponding shifts in the wrong direction. The addition of ZPVCs strengthens the correlations for **2** and **3**, but weakens them for **1** and **4**. Slopes are underestimated for every molecule, although only those for **3** and **4** have the correct sign, as does that for **1** evaluated by CCSD-MVG. All slopes for the shifts of **2** have the wrong sign, as do those of **1** for almost all methods. The addition of ZPVCs increases the slope for **3** and **4**, but the solvent shift remains underpredicted. For **1** and **2**, where calculations predict the incorrect direction of the shift, ZPVCs further increase the slope magnitude towards more negative values. This indicates that such vibrational corrections do not produce a general improvement of calculated results for the present set of target molecules.

5 | CONCLUSIONS

A detailed study has been performed to elucidate the influence of solvation effects on the dispersive optical activity of four small organic molecules: (*R*)-α-pinene (**1**), (*S*)-3-carene (**2**), (*R*)-*cis*-pinane (**3**), and (*S*)-2-chloropropionitrile (**4**). In particular, this test set was exploited to systematically examine the quality of agreement attained between experimental measurements of specific rotation, $[\alpha]_\lambda^T$, and calculations performed with PCM and three levels of theory: B3LYP, CAM-B3LYP, and CCSD, where the latter used two choices of gauge for the magnetic perturbation. In the gas phase, theory and experiment display excellent correlations, in keeping with previous reports.[49] Indeed, despite specific cases of overestimated or underestimated predictions, the relationship between theoretical and experimental rotatory powers (viz., the experiment-theory correlation) in the gas phase is strongly linear for all methods (the only exception being B3LYP results obtained for molecule **1**). Most importantly, all quantum-chemical analyses correctly reproduce the sign of the observed chiroptical response. The addition of ZPVCs tends to improve calculated gas-phase results (cf. Figure 10), favoring coupled-cluster methods (which underestimate experimental findings) at the expense of their density-functional counterparts (which overestimate experimental findings).

Experiments clearly show that solvation can have a large effect on dispersive optical activity, with each solute-solvent pair behaving differently. PCM does predict an overall effect on $[\alpha]_\lambda^T$, but its magnitude is significantly underestimated. This trend is apparent in Figures 4 and 5, where there is a large disparity among rotatory powers measured in solution, while the corresponding spread for calculations is minimal. Coupled-cluster singles and doubles with both choices of gauge underestimates the specific rotation in solution for three of the four target molecules, while overestimating the effect for **2**. On the other hand, the various functionals considered by the present work provide a somewhat mixed behavior (cf. Figures 10 and 11). For all methods, the linear-fit correlation found in the gas phase seems to deteriorate in the presence of a solvent medium. The addition of ZPVCs has a similar effect to that in the gas phase, causing the underestimated predictions for **3** and **4** to be improved while the kindred overestimated results for **1** and **2** are made worse.

Solvation shifts (cf. Equation 7) are found to be very difficult to reproduce, particularly for those cases where the magnitude of $[\alpha]_{\lambda}^{T}$ decreases in solution. Such behavior is observed for compounds **1** and **2**, and PCM is unable to reproduce these effects except in the case of **1** with CCSD-MVG. Other solution-phase calculations always give larger rotatory powers than those predicted for the gas phase, independent of the initial sign or direction of the experimental solvent shift. For molecules **3** and **4**, ZPVCs produce a minute increase towards experimental values of the solvent shift, whereas for **1** and **2** the solvent shifts tend to worsen upon incorporation of such vibrational corrections.

The emerging results suggest that it may be better to compute the value of the specific rotation in solution directly rather than attempt to obtain solvation shifts with PCM, as one may apply empirical corrections to account for any systematic offsets. However, the attendant error seems more molecule dependent than in the gas phase, as demonstrated succinctly in the case of (*S*)-3-carene (**2**). The shortcomings in PCM may reflect the fact that the current model is purely electrostatic in nature, and the missing effects of dispersion and repulsion may play an important role for chiroptical properties.[61] Additionally, the process of "chiral imprinting", as embodied in the chiral ordering induced in the achiral solvent molecules that constitute the first solvation shell, has been shown to afford significant contributions to $[\alpha]_{\lambda}^{T}$ in certain cases, and such phenomena cannot be reproduced by PCM.[23] Thus, dispersive optical-activity calculations in solution based upon the standard PCM methodology do not seem to offer the same predictive power as kindred calculations performed in the isolated-molecule limit of the vapor phase, and more sophisticated treatments of solvation appear to be necessary.

ACKNOWLEDGMENTS

T.A. and M.C. are grateful for support from the National Science Foundation under CHE-1650942. P.M.L. and P.H.V. gratefully acknowledge the support of the U.S. National Science Foundation under the auspices of grant CHE-1464957.

ORCID

Patrick H. Vaccaro http://orcid.org/0000-0001-7178-7638
Marco Caricato http://orcid.org/0000-0001-7830-0562

REFERENCES

1. Lowry TM. In: Donnan FG, ed. *Optical Rotatory Power*. London: Longmans, Green, and Co. Ltd.; 1935.
2. Polavarapu PL. Ab initio molecular optical rotations and absolute configurations. *Mol Phys*. 1997;91:551-554.
3. Cheeseman JR, Frisch MJ, Devlin FJ, Stephens PJ. Hartree−Fock and density functional theory ab initio calculation of optical rotation using GIAOs: basis set dependence. *J Phys Chem A*. 2000;104:1039-1046.
4. Grimme S. Calculation of frequency dependent optical rotation using density functional response theory. *Chem Phys Lett*. 2001;339:380-388.
5. Autschbach J, Patchkovskii S, Ziegler T, van Gisbergen SJA, Baerends EJ. Chiroptical properties from time-dependent density functional theory. II. Optical rotations of small to medium sized organic molecules. *J Chem Phys*. 2002;117:581-592.
6. Ruud K, Helgaker T. Optical rotation studied by density-functional and coupled-cluster methods. *Chem Phys Lett*. 2002;352:533-539.
7. Stephens PJ, McCann DM, Cheeseman JR, Frisch MJ. Determination of absolute configurations of chiral molecules using ab initio time-dependent density functional theory calculations of optical rotation: how reliable are absolute configurations obtained for molecules with small rotations? *Chirality*. 2005;17:52-64.
8. Grimme S, Bahlmann A, Haufe G. Ab initio calculations for the optical rotations of conformationally flexible molecules: a case study on six-, seven-, and eight-membered fluorinated cycloalkanol esters. *Chirality*. 2002;14:793-797.
9. Ruud K, Stephens PJ, Devlin FJ, Taylor PR, Cheeseman JR, Frisch MJ. Coupled-cluster calculations of optical rotation. *Chem Phys Lett*. 2003;373:606-614.
10. Tam MC, Russ NJ, Crawford TD. Coupled cluster calculations of optical rotatory dispersion of (S)-methyloxirane. *J Chem Phys*. 2004;121:3550-3557.
11. Crawford TD, Stephens PJ. Comparison of time-dependent density-functional theory and coupled cluster theory for the calculation of the optical rotations of chiral molecules. *J Phys Chem A*. 2008;112:1339-1345.
12. Pedersen TB, Koch H, Boman L, Sánchez De Merás AMJ. Origin invariant calculation of optical rotation without recourse to London orbitals. *Chem Phys Lett*. 2004;393:319-326.
13. Crawford TD, Owens LS, Tam MC, Schreiner PR, Koch H. Ab initio calculation of optical rotation in (P)-(+)-[4]triangulane. *J Am Chem Soc*. 2005;127:1368-1369.
14. Krykunov M, Autschbach J. Calculation of optical rotation with time-periodic magnetic-field-dependent basis functions in approximate time-dependent density-functional theory. *J Chem Phys*. 2005;123:114103
15. Autschbach J. Computing Chiroptical properties with first-principles theoretical methods: background and illustrative examples. *Chirality*. 2009;21:E116-E152.
16. Vaccaro PH. Optical rotation and intrinsic optical activity. In: Berova N, Polavarapu PL, Nakanishi K, Woody RW, eds. *Comprehensive Chiroptical Spectroscopy, Instrumentation, Methodologies, and Theoretical Simulations*. Vol.1 Hoboken, New Jersey: John Wiley & Sons; 2012:275-324.

17. Crawford TD, Kumar A, Hannon KP, Höfener S, Visscher L. Frozen-density embedding potentials and chiroptical properties. *J Chem Theory Comput*. 2015;11:5305-5315.

18. Wilson SM, Wiberg KB, Cheeseman JR, Frisch MJ, Vaccaro PH. Nonresonant optical activity of isolated organic molecules. *J Phys Chem A*. 2005;109:11752-11764.

19. Müller T, Wiberg KB, Vaccaro PH. Cavity ring-down polarimetry (CRDP): a new scheme for probing circular birefringence and circular dichroism in the gas phase. *J Phys Chem A*. 2000;104:5959-5968.

20. Wiberg KB, Wang Y, Murphy MJ, Vaccaro PH. Temperature dependence of optical rotation: α-pinene, β-pinene, cis--pinane, ecamphene, camphor, and fenchone. *J Phys Chem A*. 2004;108:5559-5563.

21. Wiberg KB, Wang YG, Wilson SM, Vaccaro PH, Cheeseman JR. Chiroptical properties of 2-chloropropionitrile. *J Phys Chem A*. 2005;109:3448-3453.

22. Lahiri P, Wiberg KB, Vaccaro PH. A tale of two carenes: intrinsic optical activity and large-amplitude nuclear displacement. *J Phys Chem A*. 2012;116:9516-9533.

23. Mukhopadhyay P, Zuber G, Wipf P, Beratan DN. Contribution of a solute's chiral solvent imprint to optical rotation. *Angew Chemie - Int Ed*. 2007;46:6450-6452.

24. Mukhopadhyay P, Zuber G, Goldsmith MR, Wipf P, Beratan DN. Solvent effect on optical rotation: a case study of methyloxirane in water. *Chemphyschem*. 2006;7:2483-2486.

25. Kundrat MD, Autschbach J. Ab initio and density functional theory modeling of the chiroptical response of glycine and alanine in solution using explicit solvation and molecular dynamics. *J Chem Theory Comput*. 2008;4:1902-1914.

26. Kundrat MD, Autschbach J. Modeling of the chiroptical response of chiral amino acids in solution using explicit solvation and molecular dynamics. *J Chem Theory Comput*. 2009;5:1051-1060.

27. Haghdani S, Hoff BH, Koch H, Åstrand PO. Solvent effects on optical rotation: on the balance between hydrogen bonding and shifts in dihedral angles. *J Phys Chem A*. 2017;121:4765-4777.

28. Lipparini F, Egidi F, Cappelli C, Barone V. The optical rotation of methyloxirane in aqueous solution: a never ending story? *J Chem Theory Comput*. 2013;9:1880-1884.

29. Miertuš S, Scrocco E, Tomasi J. Electrostatic interaction of a solute with a continuum. A direct utilizaion of Ab initio molecular potentials for the prediction of solvent effects. *Chem Phys*. 1981;55:117

30. Cancès E, Mennucci B, Tomasi J. A new integral equation formalism for the polarizable continuum model: theoretical background and applications to isotropic and anisotropic dielectrics. *J Chem Phys*. 1997;107:3032-3041.

31. Tomasi J, Mennucci B, Cammi R. Quantum mechanical continuum solvation models. *Chem Rev*. 2005;105:2999-3093.

32. Mennucci B, Cancès E, Tomasi J. Evaluation of solvent effects in isotropic and anisotropic dielectrics and in ionic solutions with a unified integral equation method: theoretical bases, computational implementation, and numerical applications. *J Phys Chem B*. 1997;101:10506-10517.

33. Mennucci B, Tomasi J, Cammi R, et al. Polarizable continuum model (PCM) calculations of solvent effects on optical rotations of chiral molecules. *J Phys Chem A*. 2002;106:6102-6113.

34. da Silva CO, Mennucci B, Vreven T. Density functional study of the optical rotation of glucose in aqueous solution. *J Org Chem*. 2004;69:8161-8164.

35. Stephens PJ, Devlin FJ, Cheeseman JR, Frisch MJ, Mennuci B, Tomasi J. Prediction of optical rotation using density functional theory: 6,8-dioxabicyclo[3.2.1]octanes. *J Phys Chem A*. 2000;11:2443-2448.

36. Caricato M. Implementation of the CCSD-PCM linear response function for frequency dependent properties in solution: application to polarizability and specific rotation. *J Chem Phys*. 2013;139:114103

37. Lahiri P, Wiberg KB, Vaccaro PH, Caricato M, Crawford TD. Large solvation effect in the optical rotatory dispersion of norbornenone. *Angew Chemie - Int Ed*. 2014;53:1386-1389.

38. Lahiri P, Wiberg KB, Vaccaro PH. Dispersive optical activity of (R)-methylene norbornene: intrinsic response and solvation effects. *J Phys Chem A*. 2017;121:8251-8266.

39. Ruud K, Taylor PR, Åstrand PO. Zero-point vibrational effects on optical rotation. *Chem Phys Lett*. 2001;337:217-223.

40. Wiberg KB, Vaccaro PH, Cheeseman JR. Conformational effects on optical rotation. 3-substituted 1-Butenes. *J Am Chem Soc*. 2003;125:1888-1896.

41. Mort BC, Autschbach J. Magnitude of zero-point vibrational corrections to optical rotation in rigid organic molecules: a time-dependant density functional study. *J Phys Chem A*. 2005;109:8617-8623.

42. Mort BC, Autschbach J. Temperature dependence of the optical rotation in six bicyclic organic molecules calculated by vibrational averaging. *Chemphyschem*. 2007;8:605-616.

43. Rosenfeld L. Quantenmechanische Theorie der natürlichen optischen Aktivität von Flüssigkeiten und Gasen. *Z Phys*. 1929;52:161-174.

44. Koch H, Jørgensen P. Coupled cluster response functions. *J Chem Phys*. 1990;93:3333-3344.

45. Pedersen TB, Koch H. Coupled cluster response functions revisited. *J Chem Phys*. 1997;106:8059-8072.

46. Olsen J, Jørgensen P. Linear and nonlinear response functions for an exact state and for an MCSCF state. *J Chem Phys*. 1985;82:3235-3264.

47. Crawford TD, Tam MC, Abrams ML. The problematic case of (*S*)-methylthiirane: electronic circular dichroism spectra and optical rotatory dispersion. *Mol Phys*. 2007;105:2607-2617.

48. Frisch MJ, Trucks GW, Schlegel HB, et al. *Gaussian Development Version, Revision I.09*. Wallingford CT: Gaussian Inc.; 2009.

49. Srebro M, Govind N, de Jong WA, Autschbach J. Optical rotation calculated with time-dependent density functional theory: the OR45 benchmark. *J Phys Chem A*. 2011;115:10930-10949.

50. Becke AD. A new mixing of Hartree–Fock and local density-functional theories. *J Chem Phys*. 1993a;98:1372-1377.

51. Becke AD. Density-functional thermochemistry. III. The role of exact exchange. *J Chem Phys*. 1993b;98:5648-5652.

52. Lee C, Yang W, Parr RG. Development of the Colle-Salvetti correlation-energy formula into a functional of the electron density. *Phys Rev B*. 1998;37:785-789.

53. Yanai T, Tew DP, Handy NC. A new hybrid exchange-correlation functional using the Coulomb-attenuating method (CAM-B3LYP). *Chem Phys Lett*. 2004;393:51-57.

54. Čížek J. On the use of the cluster expansion and the technique of diagrams in calculations of correlation effects in atoms and molecules. In: LeFebvre R, Moser C, eds. *Advances in Chemical Physics: Correlation Effects in Atoms and Molecules*. Hoboken, New Jersey: John Wiley & Sons; 1969:35-89.

55. Purvis GD, Bartlett RJ. A full coupled-cluster singles and doubles model: the inclusion of disconnected triples. *J Chem Phys*. 1982;76:1910-1918.

56. Scuseria GE, Janssen CL, Schaefer HF. An efficient reformulation of the closed-shell coupled cluster single and double excitation (CCSD) equations. *J Chem Phys*. 1988;89:7382-7387.

57. Scuseria GE, Schaefer HF. Is coupled cluster singles and doubles (CCSD) more computationally intensive than quadratic configuration interaction (QCISD)? *J Chem Phys*. 1989;90:3700-3703.

58. London F. Théorie quantique des courants interatomiques dans les combinaisons aromatiques. *J Phys Radium*. 1937;8:397

59. Ditchfield R. Self-consistent perturbation theory of diamagnetism. *Mol Phys*. 1974;27:789

60. Lipparini F, Scalmani G, Mennucci B, Cancès E, Caricato M, Frisch MJ. A variational formulation of the polarizable continuum model. *J Chem Phys*. 2010;133(14106):

61. Amovilli C, Mennucci B. Self-consistent-field calculation of Pauli repulsion and dispersion contributions to the solvation free energy in the polarizable continuum model. *J Phys Chem B*. 1997;101:1051-1057.

SUPPORTING INFORMATION

Additional Supporting Information may be found online in the supporting information tab for this article.

How to cite this article: Aharon T, Lemler P, Vaccaro PH, Caricato M. Comparison of measured and predicted specific optical rotation in gas and solution phases: A test for the polarizable continuum model of solvation. *Chirality*. 2018;1–13. https://doi.org/10.1002/chir.22822